

Single Magnetic Atom on a Surface: Anisotropy Energy and Spin Density

Jing-Neng Yao¹ and Chiung-Yuan Lin¹

¹*Department of Electronics Engineering and Institute of Electronics,
National Chiao Tung University, Hsinchu, Taiwan*

(Dated: July 30, 2018)

Studying single-atom magnetic anisotropy on surfaces enables the exploration of the smallest magnetic storage bit that can be built. In this work, magnetic anisotropy of a single rare-earth atom on a surface is studied computationally for the first time. The single adatom and its substrate surface are chosen to be a Dysprosium (Dy) atom and a copper-nitrite surface, respectively, where single transition-metal magnetic atoms on the same surface were previously studied one atom at a time by scanning tunneling microscopes. We propose unconventional f and d subshell symmetries so that following the first-principles calculations, simple pictorial analyses of the spin-density distribution can be performed for the first time, independently for both a rare-earth atom Dy and a transition-metal Fe. The magnetic anisotropy energy of Dy on the surface is calculated to be a factor of five larger than the previous highest one, reaching a record-high value of 31 meV.

PACS numbers:

I. INTRODUCTION

The desire of higher-density magnetic data storage is becoming more emergent to conform to the explosive growth of today's information industry. The continued downscaling of storage bits will require significant enhancement of magnetic anisotropy energy (MAE) per atom to overcome the fundamental, superparamagnetic limit. Single-atom magnetic anisotropy on surfaces serves as an important bottom-up approach of such enhancements. A surface magnetic adatom no longer has the isotropic orbital electronic structures of its free atom, and consequently its spin-orbit couplings (SOC) vary in different spin orientations. Such an anisotropy is not only technologically relevant to the smallest magnetic storage bit that can be built, but also of great scientific interest for its fascinating quantum effects¹⁻³. Pioneering experiments⁴⁻⁷ have been able to measure the MAE of single transition-metal atoms and dimers on surfaces, followed by computational studies^{4,5,8,9} that are consistent with the measurements. Among those experiments, scanning tunneling microscopes (STM) can even reach the precision such that magnetic atoms can be built, manipulated, and measured one atom at a time at desired atomic sites of a CuN surface⁵⁻⁷. There is even a very recent STM study¹⁰ that can fabricate a bistable atomic-scale antiferromagnet, which enables a low-temperature demonstration of dense nonvolatile storage of information. However, the magnetic properties of such adatoms, e.g. spin density, have not yet been understood in simple, atomic-scale microscopic pictures. Also, MAE of non-transition-metal atoms, the rare earth for example, have not been explored, and are potential candidates with even higher single-atom MAE so that one may build atomic-scale storage bits in the future.

We start this study from first-principles calculations of a single rare-earth atom Dysprosium (Dy) on a CuN surface. Analysis of subshell quantum numbers, orbital shapes, and occupations of the $4f$ orbitals leads to simple

explanation of the calculated spin-density distribution of the Dy atom. The success of such orbital analysis is then duplicated to the previously studied single Fe atom on the same surface^{5,9,11}, showing that this simple picture works independently for both the transition-metal d and rare-earth f orbitals. This work of Dy on a CuN surface is also the first study of the MAE of a single rare-earth atom on a surface, which is calculated by first principles to be a factor of five larger than the previously largest single-atom MAE, Co on the Pt surface⁸.

II. COMPUTATIONAL APPROACHES

We construct a supercell of 5-layer Cu(100) slabs, place N and Dy atoms on the surface in the same way as the density-functional-theory (DFT) studies of single Fe and Mn adatoms^{5,9,12}, and then perform DFT calculations using the basis set of all-electron full-potential linearized augmented plane wave¹³. A naive local-density or generalized-gradient approximation makes the $4f$ orbitals be pinned at the fermi level and causes a fractional $4f$ occupation, inconsistent with the photoemission measurements of rare-earth nitride bulks, and this problem was shown to be resolved by performing a DFT+U calculations instead¹⁴. To find the correct U and J values for DFT+U, we perform PBE+U calculations^{13,15-17} and inspect the $4f$ occupation number n_{4f} of Dy on the CuN surface with a series of U and J . When $J = 0$, and U ranges from 0 to 9 eV (noting that $U = 0$ denotes PBE itself), the occupation number stays at $n_{4f} = 9.6$ regardless of the U value used. This means that with solely U turned on, the unphysical fermi-level pinning of one of the f states remains the same as the naive PBE. If J is turned on to be a positive value 1.2 eV at $U = 9$ eV, the f state originally pinned at fermi-level lowers in energy, and becomes fully occupied. However, the occupation number then becomes $n_{4f} \approx 10$, inconsistent with the typical $n_{4f} \approx 9$ in either a DFT+U calcula-

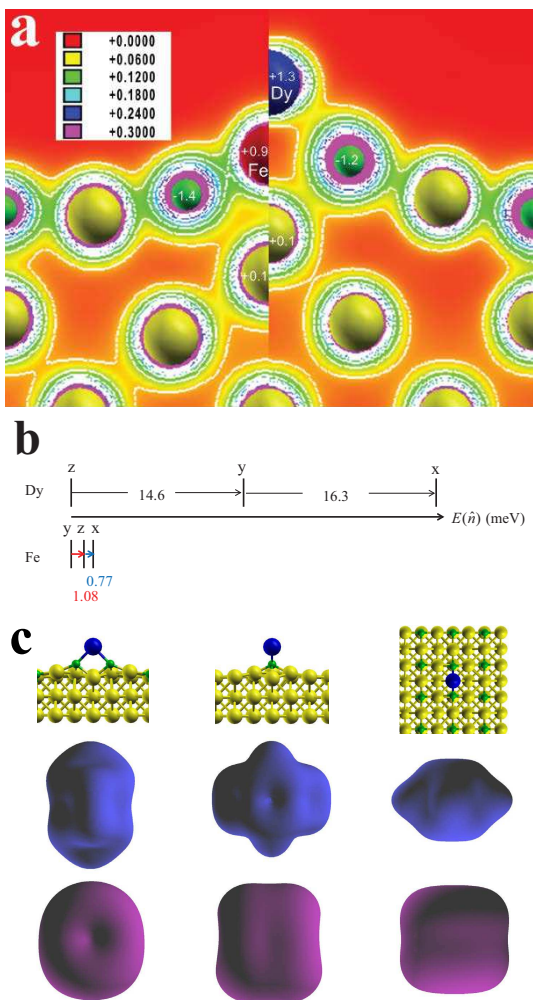


Figure 1: (a) Electron density contour of a single Dy on the CuN surface along the N-Dy-N row and the out-of-plane direction, in comparison with the Fe case⁵. The numbers inside the circles indicate the net charge on selected atoms. (b) Level diagrams in scale showing the calculated MAE of Dy and Fe on the CuN surface, respectively. The Fe case is done by Shick *et al.*⁹ (c) Calculated spin-density isosurfaces (second row, blue) of Dy on CuN at the magnitude of $0.05e/a_0^3$ within a $3 \times 3 \times 3 \text{ \AA}^3$ cube centered at the Dy nucleus, by looking (left to right) along x , y , and z directions. Each stick-ball structure corresponds to one of the three directions. The purple surfaces are the corresponding Fe spin density for comparison.

tion of a DyN bulk¹⁴ or a recent quantum-chemistry, complete active space self-consistent field (CASSCF) calculation of a DyCl₃ molecule¹⁸. If we first determine $U = 6$ eV from a constraint PBE calculation^{13,19}, and are gradually turning on a negative J , we initially find that the DFT self-consistent cycles do not converge before J reaches -0.8 eV, indicating unstable electronic structures. When J reaches -0.8 eV, the self-consistent cycles converge nicely, and give a reasonable occupation number $n_{4f} = 8.9$, consistent with the typical $4f^9$ configuration of Dy. Therefore, for Dy on the CuN surface, we

have determined that $U = 6$ eV and $J = -0.8$ eV yields a $4f^9$ configuration that agrees with both the DFT+U calculation of a DyN bulk¹⁴ and the CASSCF calculation of a DyCl₃ molecule¹⁸. Atomic charges and spins are calculated by Bader analysis²⁰.

III. RESULTS

As already pointed out in the previous Fe study⁵, when an adatom is deposited onto the Cu site of the surface, it establishes polar covalent bonds with the nearest-neighbor N atoms that replaces the original CuN binding network. The calculated electron density of a Dy atom in the CuN surface is shown in Fig. 1a, together with the previously calculated Fe re-presented. As one can see, the Dy atom, sitting even higher on top of the surface, attracts its neighboring N atoms further out of the surface than the Fe case. We have also calculated that Dy and its neighboring N are $+1.3$ and -1.2 charged respectively. Compared with the $+0.9$ and -1.4 charged Fe and its neighboring N respectively, the Dy-N bond of the Dy system has a polarity approximately the same as the Fe-N.

By pointing the Dy spin in the hollow, N-row, and out-of-plane three symmetry directions (to be called x , y , and z respectively) in our PBE+U total-energy calculations with SOC included, we obtain the Dy MAE $E(\hat{n})$ of $\hat{n} = \hat{e}_x$, \hat{e}_y , and \hat{e}_z , and compare it with the Fe case, as shown in the level diagram in Fig. 1b. One notices that in contrast to the Fe case, the most-preferred magnetization axis of Dy is oriented in the out-of-plane direction, while both atoms have their least-preferred axis pointing in the hollow direction. The MAE of Dy is basically one order of magnitude larger than that of Fe, and is five times larger than the 6meV MAE of Co on the Pt surface⁸, the largest single-atom MAE reported previously.

The previously studied Fe on the surface has 13.5% of spin density extends into the surrounding atoms with the spreading primarily along the N-row direction⁵. In contrast to Fe, when calculating Dy on the same surface, we find that a net spin of $S = 2.9$ is localized at the Dy atom, and $S = 2.9$ by including the spin of all atoms, indicating that there is no spin spreading. The $S = 2.9$ of Dy includes two parts of contribution from our analysis, $S = 2.5$ from the localized electronic configuration $(4f)^9$ (within the Dy muffin-tin sphere), and $S = 0.4$ from the delocalized $(6s5d)^1$ (out of the muffin-tin sphere but within the Bader basin), where $6s5d$ denotes a hybridized molecular orbital²¹. The significant reduction of spin spreading when replacing Fe by Dy is obviously because the Dy $4f$ orbitals are more localized than the Fe $3d$. Another interesting feature is the shape of the spin density. When looking closely at the spin isosurfaces of the Dy and Fe atoms along all three crystal-symmetry directions in Fig. 1c, the shapes of Dy and Fe are found to be approximately a hexagon and a square, respectively, along either the N-row or out-of-plane direction, while

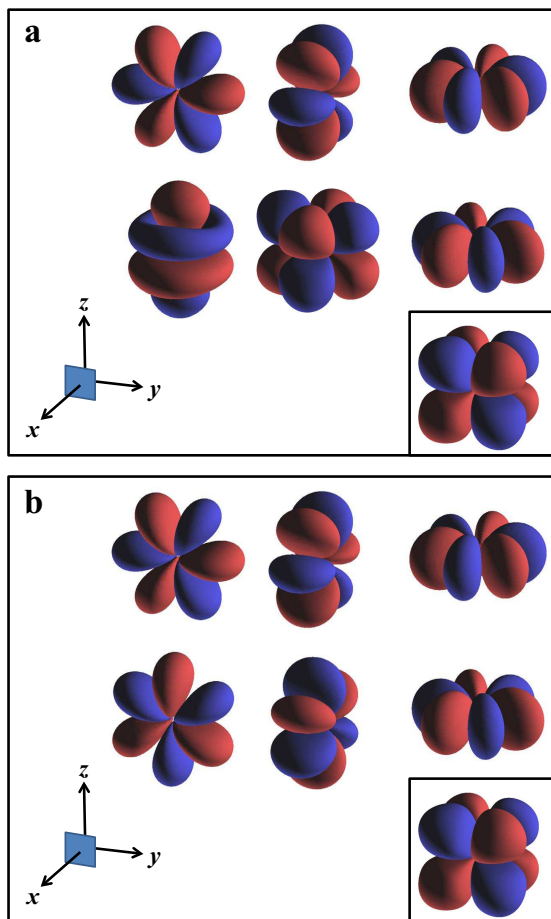


Figure 2: Schematic plots of two different sets of 4f orbitals, where blue (red) zones denote positive (negative) values. (a) The general set²², from left to right: (upper) yz^2 , $z(z^2 - 3x^2)$, $x(x^2 - 3y^2)$, (lower) z^3 , $z(x^2 - y^2)$, $y(3x^2 - y^2)$. The xyz orbital is plotted in the inset at the right-lower corner. (b) The $|L_i|$ -fully-polarized set, from left to right: (upper) yz^2 , $z(z^2 - 3x^2)$, $x(x^2 - 3y^2)$, (lower) zy^2 , xz^2 , $y(3x^2 - y^2)$. All six orbitals have a unique six-petal shape. The only exceptional shape of the xyz orbital is plotted in the inset at the right-lower corner.

both atoms become more round-shape-like along the hollow. This seemingly mysterious observation of spin shapes will become clear when we later look into the Fe 3d and Dy 4f orbitals in the CuN surface.

The d orbitals in a crystal environment have the following well-known subshell symmetries, z^2 , $x^2 - y^2$, xy , yz , zx . The exotic, complicated f orbitals, which are rarely shown in literatures, have two commonly used sets of subshell symmetries, the cubic and the general sets²². As an example, we plot the 4f general set in Fig. 2a. We find there are four orbitals having a unique six-petal shape: yz^2 , $z(z^2 - 3x^2)$, $x(x^2 - 3y^2)$, and $y(3x^2 - y^2)$, and are different from the rest three. The six-petal shape suggests that the hexagonal spin density is related to the 4f orbitals in some way. However, the z^3 and $z(x^2 - y^2)$ orbitals that do not have six-petal shapes prevent us from

establishing a relation between the spin density and the general-set 4f orbitals. Here we propose an unconventional set of f orbitals such that six of the orbitals have fully polarized angular momenta $|L_i|$, as one will see its advantages in the orbital analysis of the spin shapes. Five out of the seven orbitals, xz^2 , yz^2 , $y(3x^2 - y^2)$, $x(x^2 - 3y^2)$, and xyz still belong to the general set. The rest two are $z(z^2 - 3x^2)$ and zy^2 , which are related to the general-set orbitals z^3 and $z(x^2 - y^2)$ simply by the following orthogonal transformation

$$\begin{aligned} \begin{pmatrix} |x'(x'^2 - 3y'^2)\rangle \\ |x'z'^2\rangle \end{pmatrix} &= \begin{pmatrix} |z(z^2 - 3x^2)\rangle \\ |zy^2\rangle \end{pmatrix} \\ &= \frac{1}{4} \begin{pmatrix} \sqrt{10} & -\sqrt{6} \\ -\sqrt{6} & -\sqrt{10} \end{pmatrix} \begin{pmatrix} |z^3\rangle \\ |z(x^2 - y^2)\rangle \end{pmatrix}, \end{aligned} \quad (1)$$

where the primed coordinates are arranged as $(x', y', z') = (y, z, x)$. It can be seen that $z(3y^2 - z^2)$ and zx^2 , which are orthogonally transformed from the general-set z^3 and $z(x^2 - y^2)$, no longer belong to the general set in the unprimed coordinates, but are actually the general-set orbitals $x'(x'^2 - 3y'^2)$ and $x'z'^2$ in the primed coordinates. One can easily verify that each orbital of this set except for xyz , with its quantization axis \hat{n} properly chosen along one coordinate axis x_i , has its angular momentum fully polarized, that is, they are eigenstates of $|\mathbf{L} \cdot \hat{e}_i| = |L_i|$ with eigenvalues $|m| = 3 = l$. Due to the reflection symmetry of these orbitals in the $\pm \hat{e}_i$ directions, their angular-momentum polarization has a sign ambiguity. The full polarization of $|L_i|$ of these six 4f orbitals can be further visualized clearly by looking at their orbital shapes. As one can see in Fig. 2b, the above mentioned six fully-polarized 4f orbitals have a unique six-petal shape, and can be grouped into three pairs. Each pair of orbitals have the same coordinate axis as their central symmetry axis, and are related to each other by exchanging their in-plane axes. The most obvious full polarization can be realized for the $y(3x^2 - y^2)$ and $x(x^2 - 3y^2)$ orbitals, which are eigenstates of $|L_z|$ with eigenvalues $|m| = 3$, and have z as their central axis. Similarly, each of the rest four fully-polarized orbitals have their central axes as their polarization directions. The only exception, the xyz orbital, has eight lobes pointing to the corners of a cube.

Our calculations show that the Dy 4f majority-spin states are all fully occupied and are very low-lying, extremely atomic-like levels. The orbital analysis of this work does not depend on the details of the Dy 4f majority-spin states as long as all of them are fully occupied, and their details are not presented here. For minority-spin states, we plot their PDOS in Fig. 3a, and find that xz^2 and $y(3x^2 - y^2)$ are mainly occupied, and yz^2 and $x(x^2 - 3y^2)$ slightly occupied. The occupation numbers of the rest of the 4f minority-spin states are negligible. The 5d6s electron mentioned in a previous paragraph is mostly delocalized out of the Gd muffin-tin sphere, and has a negligible PDOS within that sphere.

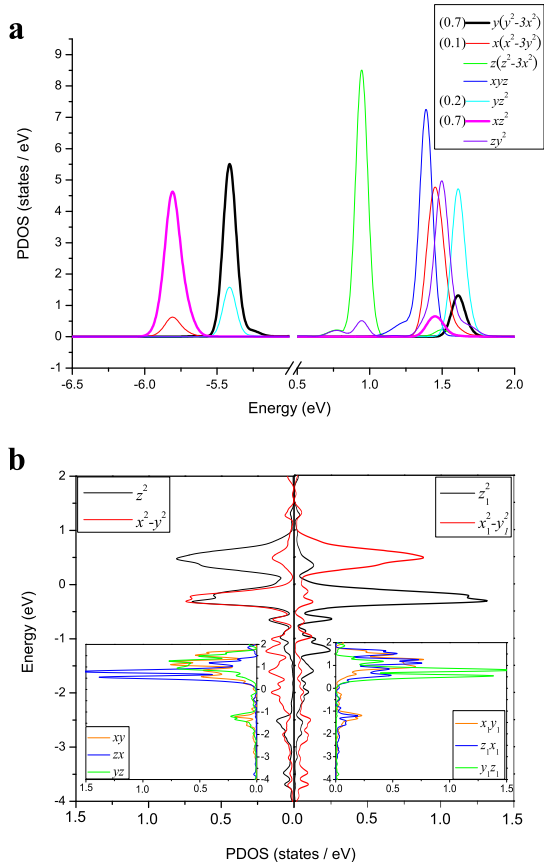


Figure 3: (a) The 4*f* minority-spin PDOS of Dy on the CuN surface without SOC. The subshells follow the choice of Fig. 2b. The nontrivial occupation are specified in parentheses. (b) The 3*d* minority-spin PDOS of Fe on the CuN surface. The left figure has the conventional quantization axes with the hollow, N-row, and out-of-plane directions being x , y , and z axes, respectively^{9,11}. In contrast to the conventional set of axes, the right one has unconventional axes $(x_1, y_1, z_1) = (y, z, x)$, and is used to perform orbital analysis in this work for its simple occupation numbers (either nearly occupied or almost empty). The PDOS of three of the subshells are plotted separately in each inset solely for the purpose that all PDOS are better visualized.

The Dy 4*f* orbitals are rather localized as indicated from a previous paragraph that they have an approximate 0.4 Å radius. It is a good approximation to think of these orbitals in the way of electronic configurations of an atom, and therefore the nontrivial occupation (neither fully occupied nor completely empty) is determined for each orbital from the area under the curve below the Fermi level. The PDOS thus implies an approximately 4*f*⁹ configuration for the Dy atom itself.

The conventional quantization axes of the Fe 3*d* PDOS are oriented in the way that the x axis points along the hollow direction, y along the N row, and z out of plane. Such PDOS have been presented in Ref.^{9,11}, and show that all the majority-spin states are fully occu-

ped. We re-calculate the PDOS and plot the minority spins in Fig. 3b. The minority-spin PDOS show that $x^2 - y^2$ is fully occupied, z^2 partially occupied, and the rest three minority-spin states basically empty. The partially occupied spin-minority z^2 prohibits us from establishing a simple picture of either the spin-density shape or the SOC. However, one may notice that the z^2 and $x^2 - y^2$ PDOS profiles depend nontrivially on the choice (or interchange) of the coordinate axes, while the xy , yz and zx (see the insets of Fig. 3b) have trivially the same set of PDOS profiles with interchange of PDOS labels corresponding to the interchange of the coordinate axes. Therefore we search for z^2 and $x^2 - y^2$ minority-spin PDOS of all three possible assignments of coordinate axes, i.e., the hollow, N-row, and out-of-plane directions are x , y , and z axes, respectively, and the cyclic permutations. In all three axis assignments, all the majority-spin states are always fully occupied, and the xy , yz and zx minority-spin always empty, while the z^2 and $x^2 - y^2$ minority-spin states have specially simple occupations as shown in Fig. 3b under a particular assignment of new axes: the hollow, N-row, and out-of-plane directions are z_1 , x_1 , and y_1 axes, respectively. In this new coordinate system, only the z_1^2 (or equivalently x^2 in the old coordinates) orbital has paired spins, while the rest four all unpaired.

IV. DISCUSSION

With the orbital quantum numbers and occupation numbers determined, we now try to explain the spin-density shape of a Dy atom on the CuN surface. By starting with the top view, one notices that the $x(x^2 - 3y^2)$ and $y(3x^2 - y^2)$ orbitals both have the six-petal shapes centered about the z -axis. As we have identified from the PDOS analysis that $y(3x^2 - y^2)$ has roughly paired spins, while $x(x^2 - 3y^2)$ has roughly an unpaired spin. The spin density shape along the xy plane are therefore dominated by the $x(x^2 - 3y^2)$ majority spin alone. Observing the shape of the $x(x^2 - 3y^2)$ orbital, one then realizes that the hexagonal shape of the Dy spin density from a top view in Fig. 1c is essentially the consequence of the unpaired $x(x^2 - 3y^2)$ orbital (see Fig. 4a). Similarly, the $z(z^2 - 3x^2)$ and xz^2 orbitals, both with a six-petal shape centered about the y -axis, contribute to the hexagonal spin density by looking along the y direction. However, the yz^2 and zy^2 orbitals, centered about the x -axis, both have unpaired spins. Their two six-petal shapes with 30° relative to each other result in a slightly-round-shape spin-density by looking along the x direction. We can even further understand the unique dent at the y ends of the spin isosurface by the following analysis. The only unpaired orbital that carries a lobe in the y direction is yz^2 , as can be seen in Fig. 4a, and all the rest have nodes along y . On the other hand, both the other two axes receive lobe contribution from two unpaired-orbitals, e.g., $x(x^2 - 3y^2)$ and zy^2 both contribute lobes along x . Con-

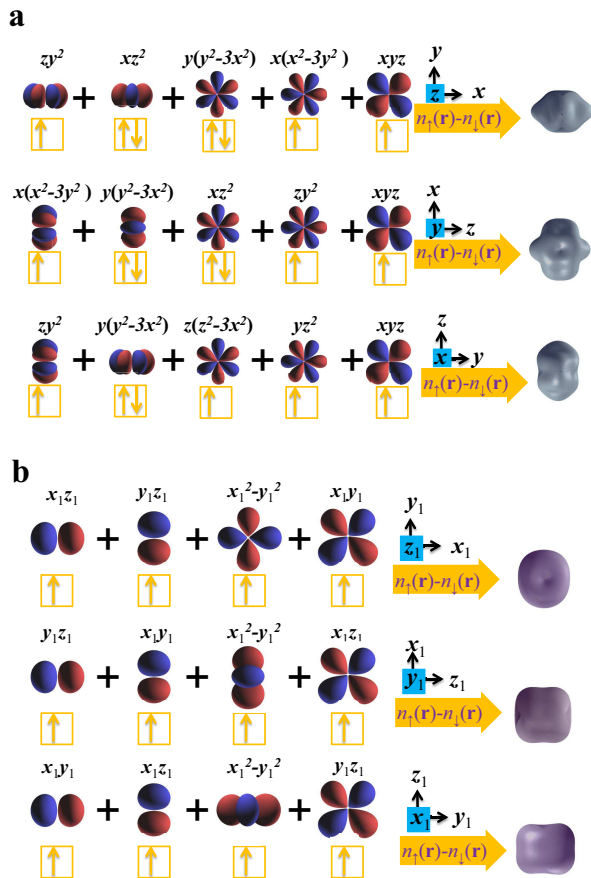


Figure 4: Illustration of how analyses of localized orbitals explain the shapes of the spin density of (a) a Dy atom on the CuN surface, and (b) Fe on the same surface. In both cases, all spin up states are occupied, and the spin-down occupation of each orbital is determined by the PDOS in Fig. 3.

sequently, the spin isosurface shrinks in the y direction due to relatively less lobe contribution than the x and z directions.

The simple occupation picture of the adatom's localized orbitals that explains the spin-density shape works not only for the rare-earth atom Dy. As we are going to show below, the same picture also works for the previously studied Fe adatom. When showing the Fe PDOS in both the conventional quantization axes (hollow x , N-row y , and out-of-plane z) and the unconventional ones (hollow z_1 , N-row x_1 , and out-of-plane y_1) in Fig. 3b, we have demonstrated that in the new coordinate system (x_1, y_1, z_1), only the z_1^2 orbital has paired spins, while the rest four are all unpaired. As seen from Fig. 4b, the square spin-density shapes of Fe in the CuN surface from the top view and N-row side view are essentially con-

sequences of the spin-unpaired z_1x_1 and y_1z_1 orbitals, respectively, while the round shape from the hollow-site side view is the combination of the spin-unpaired $x_1^2 - y_1^2$ and x_1y_1 orbitals. One also notice that the spin isosurface has a dent only at the z_1 ends. Similar to the way of explaining the Dy spin-isosurface dent, such a dent is the consequence that both the x_1 and y_1 ends have lobe contributions from the $x_1^2 - y_1^2$ orbital, while z_1 has no lobe contribution mainly due to the fact that the z_1^2 orbital is spin-paired.

V. CONCLUSION

The STM moving-atom technique has demonstrated its capability of building, manipulating, and measuring a single atomic spin in a well-characterized environment. First-principles calculations conclude that such an atomic spin forms a surface-embedded molecular magnetic structure⁵, as well as, reproduce the measured magnetic anisotropy axes⁹. As an ongoing study of the STM-engineered adatoms, this work is the first attempt to understand the spin density of a surface magnetic atom in a simple, atomic-scale microscopic picture. This is achieved by analyzing the occupations, shapes, and angular momenta of its individual localized orbitals. These localized orbitals include both the well-known d orbitals of the transition-metal atoms and the nontrivial f of the rare-earth. We determine an unconventional set of $4f$ subshell quantum numbers and an unconventional set of $3d$ quantization axes that can be used to analyze the shape of the spin density. The spin-density shape of a magnetic adatom is explained by simply counting the occupation of each individual subshell and spin state of the atom's localized orbital. These studies provide an important microscopic picture of the atomic-scale origins of magnetization distribution. We have also done the first computational study of a single rare-earth atom on a surface. The calculation predicts a record-high MAE of 31 meV. All these theoretical and computational realizations, combined with continuing experimental innovations¹⁰, may lead to further engineering of the single-atom magnetic anisotropy, further exploration of the smallest magnetic storage bit, and new fascinating applications of atomic-scale magnetism.

We thank A. Heinrich, B. Jones, and D. Rugar for stimulating discussions. We appreciate valuable technical support from J. L. Li. We acknowledge financial supports from the Taiwan National Science Foundation, the Taiwan Ministry of Education, and the Taiwan National Center for Theoretical Sciences. We also acknowledge the support of computing facilities provided by the Taiwan National Center for High-performance Computing,

¹ J. R. Friedman, M. P. Sarachik, J. Tejada and R. Ziolo, Phys. Rev. Lett. **76**, 3830 (1996).

² L. Thomas, F. Lioni, R. Ballou, D. Gatteschi, R. Sessoli

- and B. Barbara, *Nature* **383**, 145 (1996).
- ³ W. Wernsdorfer and R. Sessoli, *Science* **284**, 133 (1999).
 - ⁴ P. Gambardella *et al.*, *Science* **300**, 1130 (2003).
 - ⁵ C. F. Hirjibehedin *et al.*, *Science* **317**, 1199, (2007).
 - ⁶ A. F. Otte *et al.*, *Nature Physics*, **4**, 847, (2008).
 - ⁷ Loth, S.; Etzkorn, M.; Lutz, C. P.; Eigler, D. M.; Heinrich, A. J. *Science* **2010**, 329, 1628, (2010) .
 - ⁸ B. Lazarovits, L. Szunyogh and P. Weinberger, *Phys. Rev. B* **67**, 024415, (2003).
 - ⁹ A. B. Shick, F. Maca and A. I. Lichtenstein, *Phys. Rev. B* **79**, 172409, (2009).
 - ¹⁰ S. Loth, S. Baumann, C. P. Lutz, D. M. Eigler, A. J. Heinrich, *Science* **335**, 196 (2012).
 - ¹¹ R. Žitko and T. Pruschke, *New J. Phys.* **12**, 063040, (2010).
 - ¹² C. Y. Lin and B. A. Jones, *Phys. Rev. B* **83**, 014413, (2011).
 - ¹³ P. Blaha, K. Schwarz, G. Madsen, D. Kvasnicka, and J. Luitz, Computer code WIEN2k: An Augmented Plane Wave plus Local Orbitals Program for Calculating Crystal Properties. (Vienna University of Technology, 2001).
 - ¹⁴ P. Larson, W. R. L. Lambrecht, A. Chantis and M. Schilfgaarde, *Phys. Rev. B* **75**, 045114, (2007).
 - ¹⁵ Anisimov, V. I.; Solovyev, I. V.; Korotin, M. A.; Czyzyk, M. T.; Sawatzky, G. A. *Phys. Rev. B* **1993**, 48, 16929, (1993) .
 - ¹⁶ A. I. Liechtenstein, V. I. Anisimov and J. Zaanen, *Phys. Rev. B* **52**, R5467, (1995).
 - ¹⁷ J. P. Perdew, K. Burke and M. Ernzerhof, *Phys. Rev. Lett.* **77**, 3865, (1996).
 - ¹⁸ G. Lanza, Z. Varga, M. Kolonits and M. Hargittaia, *J. Chem. Phys.* **128**, 074301, (2008).
 - ¹⁹ G. K. H. Madsen and P. Novak, *Europhys. Lett.* **69**, 777, (2005).
 - ²⁰ R. F. W. Bader *Atoms in Molecules a Quantum Theory*, (Clarendon Press, Oxford, 1990).
 - ²¹ The Dy *4f*, *5d*, and *6s* have radii of 0.4, 1.4, and 2.0Å, respectively. As a result, the *4f* contributes a much larger radial part $dV(r)/dr$ to the SOC than *6s5d*. In fact, the *6s5d* orbital is mainly distributed out of the Dy muffin-tin sphere, and its SOC is not included in this calculation.
 - ²² See, for example, <http://winter.group.shef.ac.uk/orbitron>